A multi-objective stochastic optimization model for combined heat and power virtual power plant considering carbon recycling and utilizing

Fuqiang Zhang[1], Yichun Gong[1], Xiangcheng Zhang[2], Fei Liu[2] and Qingqing Zhou[3]*

[1]State Grid Energy Research Institute Co., Ltd., Beijing, China, [2]Economic and Technological Research Institute of State Grid Qinghai Electric Power Company, Xining, Qinghai, China, [3]School of Economics and Management of North China Electric Power University, Beijing, China

In order to give full play to the energy supply potential of distributed energy resources, this paper studies the scheduling optimization of CHP-VPP. First, the CHP unit and various distributed energy sources are aggregated into VPP. Carbon recycling and utilizing are realized through carbon capture and power-to-gas devices. At the same time, carbon storage and hydrogen storage devices are added to decouple carbon capture and P2G procedures. Then, the risk of VPP real-time scheduling is quantified through uncertainty scenario generation and CVaR. Finally, with the goals of operating cost, carbon emission, and operation risk, a multi-objective stochastic scheduling optimization model of VPP is constructed, and the subjective and objective ensemble weighting method is used to solve the problem. The example results show that the proposed method can boost the wastage of wind and photovoltaic power, and also lower the carbon emissions of VPPs.

KEYWORDS

virtual power plant (VPP), combined heat and power (CHP), carbon capture, power to gas (P2G), conditional value at risk (CVaR)

1 Introduction

The scale of distributed energy resources on the demand side has grown rapidly over the years. Due to its high energy efficiency, less pollution, and strong flexibility, it will be the key to alleviating China's energy shortage. Aiming at the problems of small capacity, large quantity and uneven distribution of distributed energy resources, virtual power plants (VPP) use advanced communication technology to realize the aggregation of different distributed energy sources, which can effectively play the spatiotemporal complementary ability of various resources and fully tap the energy supply potential of distributed energy resources.

From another perspective, multi-energy complementarity is the general trend of the future development of the energy field. And electricity and heat as the two main forms of user energy consumption, whose coupling degree will continue to deepen. In this context, some scholars put forward the concept of the combined heat and power-virtual power plant (CHP-VPP), aiming to realize the cooperative optimal scheduling of electricity and heat

through electrothermal coupling equipment such as the combined heat and power (CHP) units and electric boilers with the advanced communication and control technology of virtual power plants. At present, many scholars have studied the combined heat and power virtual power plant. Yang H studied cogeneration virtual power plants that include thermal power plants, wind farms, photovoltaic power plants, and electric boilers (Yang et al., 2024). Basu M integrated consideration of electrical, thermal, and cold requirements, improve the flexibility and economy of the system (Basu, 2023). Feng Y studied the virtual power plant coupling multiple resources of electricity, heat and gas to reduce the cost of the system (Feng et al., 2023). Some scholars have installed heat storage tanks to absorb wind power in thermoelectric joint virtual power plants and established a VPP dispatching optimization algorithm with the purpose of maximizing economic benefits (Schulz et al., 2005; Xia et al., 2016; Nazari-Heris et al., 2018). The above literature only focuses on the economic benefits of VPP, but in the context of the "Dual carbon" goal, carbon emissions will be a key indicator of optimal scheduling of virtual power plants. How to realize low carbon operation of VPP while giving full play to the potential of VPP energy supply is the main issue in the field of VPP research.

In the above context, the progress of carbon capture and Power-to-gas (P2G) technology provides an effective way for the green development of VPP. Tan C studied carbon capture units, which promoted the consumption of electricity from virtual power plants, and made the carbon emission reduction effect more significant (Tan et al., 2021). Ju L studied power-to-gas devices to absorb excess wind and solar power generation and convert CO_2 into CH_4, effectively reducing the carbon emissions of VPP (Ju et al., 2019). Babaee S studied CO_2 recycling through Gas-power Plant Carbon Capture (GPPCC) and P2G (Babaee and Loughlin, 2018). Zhu C studied a carbon storage device to decouple the capture and treatment process of CO_2 (Zhu et al., 2023), and Wang C studied a hydrogen storage device to decouple the production and consumption process of H_2 (Wang et al., 2024). The above literature does not consider the influence of the coupling operation mode of GPPCC and P2G on the degree of carbon cycling. However, the carbon storage device can decouple the CO2 capture and treatment process (Smit et al., 2014), and the hydrogen storage device can decouple the H2 production and consumption process (Gorre et al., 2020). In addition, many scholars ignore the uncertainties of renewable energy when they study the reduction of carbon emissions by VPP. Therefore, in this paper, the above characteristics of carbon storage device and hydrogen storage device are used to flexibly control the two gas raw materials required for methanation process. The purpose of renewable energy time shift is realized, and the degree of carbon recycling of GPPCC and P2G is improved. At the same time, under the premise of improving the economy of the system, the carbon emission reduction potential is maximized. Moreover, uncertainty processing methods such as scenario generation (SG) and conditional value at risk (CVaR) theory are introduced to enable VPP to deal with the volatilities of scenery while reducing carbon emission.

In response to the above problems, this paper uses proposes an optimal dispatching method for a combined heat and power VPP that considers carbon capture and electricity-to-gas conversion. The CHP unit and various distributed energy sources on the user side are aggregated into CHP-VPP. Then, GPPCC and P2G are used to realize carbon recycling, and the carbon and hydrogen storage devices are used to decouple the carbon capture and water electrolysis process, at the same time, the time shift of renewable energy power is realized. In addition, SG and CVaR theory are used to quantify the risk of VPP real-time scheduling. Finally, taking operation cost, carbon emission, and operation risk as optimization objectives, a virtual power plant multi-objective stochastic dispatching optimization model is constructed. The comparison between this paper and published studies is shown in Table 1.

2 Structure and operating model of virtual power plant

In Section 2 of this paper, the material or energy input and output models of components of virtual power plant are introduced, aiming at clarifying the energy or material flow relationship between components.

2.1 Structure of virtual power plant

The combined heat and power virtual power plant mainly includes a distributed electrical/thermal output module and a carbon recycling module. Among them, the distributed electrical/thermal output module includes distributed wind power, distributed photovoltaic, electric boiler, and controllable load. The carbon recycling module includes CHP unit, GPPCC, P2G, and carbon storage and hydrogen storage devices, which can recycle CO_2 generated by the CHP unit. Besides, GPPCC includes carbon capture and carbon storage. The VPP dispatching center will predict the available energy output in advance, obtain the operating status of each unit, and formulate an electric heating cooperative dispatching plan for VPP. In addition, VPPs can interact with power grids to fill power supply gaps or sell surplus power. The energy or material flow relationships between the components of VPP is shown in Figure 1.

2.2 Operating model of virtual power plant

In this paper, VPP mathematical model including CHP, P2G, GPPCC and other components is established. In addition, a multi-objective optimization model considering operational cost, carbon emission and operational risk is constructed. By solving the optimization model, the optimization objectives of VPP such as reducing carbon emission, reducing operation cost and optimizing power generation plan can be achieved, so as to make the operation of power system more efficient, stable and reliable.

TABLE 1 Comparing this work with recent research.

Ref	VPP			Uncertainty		Uncertain modeling methods
	Electrical output module	Thermal output module	Carbon recycling module	Wind	PV	
Xia et al. (2016)	√	√	×	×	×	×
Nazari-Heris et al. (2018)	√	√	×	×	×	×
Tan et al. (2021)	√	×	√	×	×	CVaR
Ju et al. (2019)	√	×	√	√	√	Ro
Babaee et al. (2020)	√	×	√	×	×	×
Yang et al. (2024)	√	√	√	√	√	CVaR
This work	√	√	√	√	√	SG-CVaR

FIGURE 1
Energy flow of VPP.
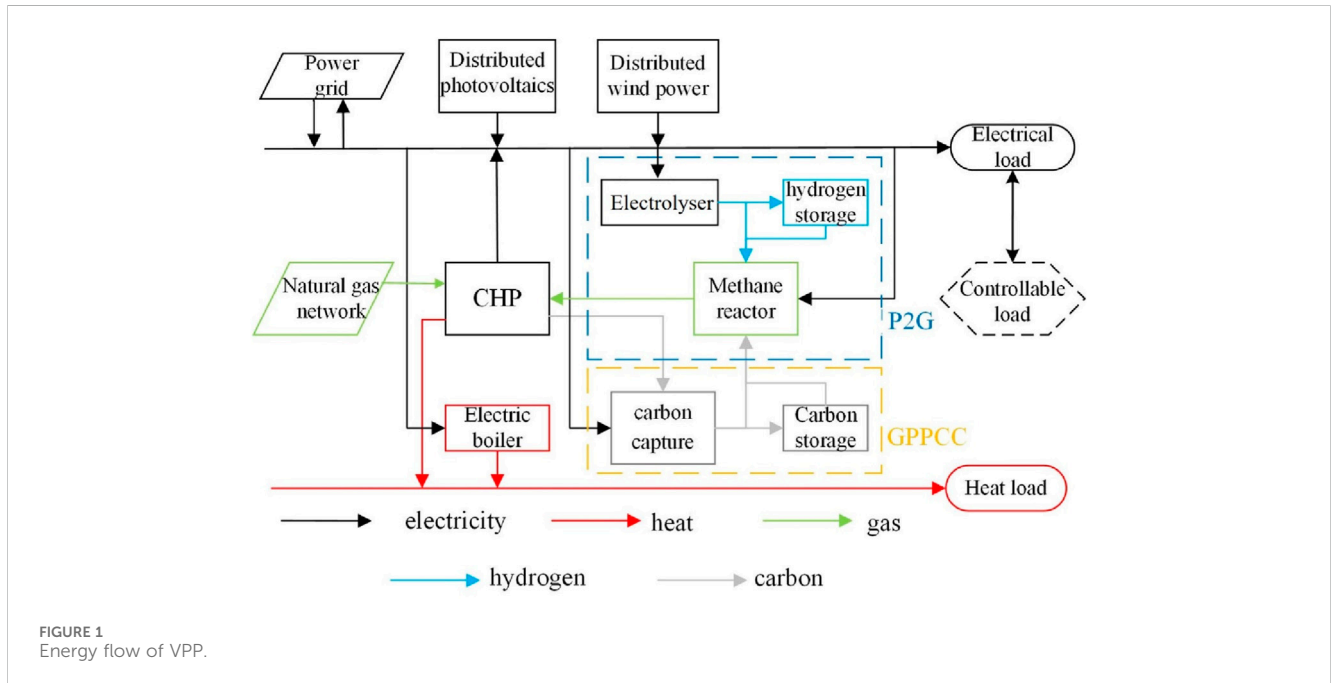
2.2.1 Distributed power/heat output module

Distributed electrical/thermal output module includes distributed wind/Photovoltaic (PV), electric boilers, and controllable loads.

(1) Distributed wind/PV

Based on the predicted wind power output, the VPP will develop an output plan for the internally distributed wind power, which satisfies the following relationships listed in Equation 1:

$$0 \le g_{WPP,t} \le g_{WPP,t}^f \tag{1}$$

Where, $g_{WPP,t}$ and $g_{WPP,t}^f$ are the planned output and predicted output of wind power at time t. The actual available output of wind power is calculated by Equation 2:

$$g_{WPP,t}^{re} = g_{WPP,t}^f + \Delta g_{WPP,t}^f \tag{2}$$

Where, $g_{WPP,t}^{re}$ and $\Delta g_{WPP,t}^f$ are the actual output and forecast error of wind power at time t. When the scale of wind power is large and geographically distributed, the prediction error can be considered to follow the normal distribution of $(0, \sigma_t^W)$, and the calculation method of σ_t^W is as shown in Equation 3 (Higgins et al., 2014):

$$\sigma_t^W = \frac{1}{5} g_{WPP,t}^f + \frac{1}{50} W_{WPP} \tag{3}$$

Where, W_{WPP} is the total installed cubage of wind turbines.

The modeling of distributed PV is consistent with that of distributed wind power, and the possibility distribution function of PV prediction error is referenced (De Giorgi et al., 2015).

(2) Electric boilers

The electric boilers can supply heat to the system with the help of the wind-wind output, and the relationship between the heat production power $h_{eb,t}$ and the power consumption power $g_{eb,t}$ is as shown in Equation 4:

$$h_{eb,t} = \omega_{eb} g_{eb,t} \tag{4}$$

Where, ω_{eb} is the electric heating efficiency of the electric boiler.

(3) Controllable loads

Customers can sign a contract with a VPP to increase their electricity consumption during valley hours or reduce it during peak hours, and receive certain compensation (Hao et al., 2023) as shown in Equation 5:

$$\Delta L_{I,t} = \sum_{k=1}^{N_I} \left(\mu_{k,t}^u \Delta L_{k,t}^u + \mu_{k,t}^d \Delta L_{k,t}^d \right) \tag{5}$$

Where, $\Delta L_{I,t}$ is the controllable load response quantity at time; N_I is the number of users; $\Delta L_{k,t}^u$ and $\Delta L_{k,t}^d$ contribute to the positive/negative response provided by the k user; $\mu_{k,t}^u$ and $\mu_{k,t}^d$ represent the state of the positive/negative response force and are 0–1 variables.

2.2.2 Carbon recycling and utilizing module

The carbon recycling module includes CHP unit, GPPCC, P2G, and gas storage units.

(1) CHP unit

In this paper, the extraction type CHP unit is used to extract part of steam from the two stages of the steam turbine as a heat source for external heating, and its feasible region is represented as shown in Equation 6 (Banadkouki, 2023; Zhang et al., 2024):

$$\begin{cases} 0 \le P_{CHP} \le C_{CHP}^e, 0 \le \phi_{CHP} \le C_{CHP}^h \\ k_m \phi_{CHP} \le P_{CHP} \le C_{CHP}^e - k_u C_{CHP}^h \end{cases} \tag{6}$$

Where, P_{CHP} is the power of CHP; C_{CHP}^e and C_{CHP}^h are rated electric and thermal power of CHP unit, respectively; ϕ_{CHP} denotes the thermal power of CHP; k_m and k_u are minimum and maximum thermoelectric ratio of CHP, respectively.

The CO_2 produced and natural gas consumed by the unit are shown in Equation 7 (Zhang et al., 2022):

$$\begin{cases} Q_{G,c,t} = e_G g_{G,t} \\ V_{CH_4,t} = \dfrac{3.6 g_{G,t}}{\eta_G H_{CH_4}} \end{cases} \tag{7}$$

Where, $Q_{G,c,t}$ and $V_{CH_4,t}$ are the mass of CO_2 produced and the volume of natural gas consumed, respectively; e_G is carbon emission intensity; $g_{G,t}$ is the total electrical power of CHP; η_G is the power generation efficiency of CHP unit; H_{CH_4} is the low calorific value of natural gas; 3.6 is the unit conversion coefficient.

(2) GPPCC

In order to better control the operation of GPPCC, this paper defines two indicators with reference to Ref. (Bassano et al., 2020):

flue gas diversion ratio $\lambda_{c,t}$ and operation energy consumption $g_{OP,t}$ which respectively represent the ratio of the flue gas flow rate diverted into GPPCC to the total flue gas flow rate generated by power generation and the variable energy consumption of GPPCC. The flow direction of CO_2 in GPPCC is as follows:

$$\begin{cases} Q_{c,t} = \lambda_{c,t} Q_{G,c,t} \\ Q_{c,t}^c = \eta_c Q_{c,t} \\ Q_{c,t}^s = Q_{G,c,t} - Q_{c,t}^c \end{cases} \tag{8}$$

Where, $Q_{c,t}$, $Q_{c,t}^c$ and $Q_{c,t}^s$ represent CO_2 being processed, successfully captured, and released into the atmosphere by GPPCC, respectively; η_c is the constant representing the CO_2 capture rate of GPPCC.

The energy consumption of GPPCC can be calculated as shown in Equation 9:

$$g_{GPPCC,t} = g_A + g_{OP,t} = g_A + \theta_{ce} Q_{c,t} \tag{9}$$

Where, g_A is the fixed energy absorbed of carbon capture, which can be regarded as a constant value due to its relatively small proportion; θ_{ce} is the power consumed per unit of CO_2. For ease of calculation, replace $Q_{c,t}^c$ with the volume $V_{c,t}^c$ in the standard case as shown in Equation 10.

$$V_{c,t}^c = Q_{c,t}^c / \rho_c \tag{10}$$

Where, ρ_c is the density of CO_2 under the standard condition.

In addition, a carbon storage device is added to the GPPCC to store part of the CO_2, generated by the unit when the renewable energy output is low, so as to realize the decoupling of carbon capture and the electron-to-gas procedure. The relationship between CO_2 captured by GPPCC and CO_2 consumed by P2G is as shown in Equation 11:

$$\begin{cases} V_{c,t}^c = V_{c,t}^{in} + V_{c,t}^{c-m} \\ V_{c,t}^m = V_{c,t}^{out} + V_{c,t}^{c-m} \end{cases} \tag{11}$$

Where, $V_{c,t}^{in}$、$V_{c,t}^{out}$ and $V_{c,t}^{c-m}$ represent CO_2 from GPPCC into the carbon storage unit, from the carbon storage unit into P2G, and directly from GPPCC into P2G, respectively; $V_{c,t}^m$ is the total amount consumed by P2G.

(3) P2G

P2G technology is mainly divided into two types: electric to hydrogen and electric to natural gas. Electric to hydrogen is electrolysis of water to generate hydrogen and oxygen. Subsequently, water and methane are generated through Sabatier catalytic reaction. Based on the idea of cascade utilization of energy, the electric to gas system helps the consumption of renewable energy, and the energy conversion efficiencies are 75%–85% and 75%–80%, respectively (Marzi et al., 2023). The energy conversion procedure is shown as Equation 12:

$$\begin{cases} V_{H_2,t} = 3.6 \eta_{H_2} g_{H_2,t} / H_{H_2} \\ V_{H_2,t}^m = g_{CH_4,t}^m / \theta_{CH_4}^m \end{cases} \tag{12}$$

Where, $V_{H_2,t}$ and $V_{H_2,t}^m$ represent H_2 produced by electrolytic water and consumed by methanation, respectively; η_{H_2} is the efficiency of converting electricity to hydrogen; H_{H_2} is the

calorific value of hydrogen; $\theta_{CH_4}^m$ is the power consumption per unit H_2 of methanation consumption; $g_{H_2,t}$ and $g_{CH_4,t}^m$ are the power consumption of water electrolysis and methanation, respectively.

In addition, a hydrogen storage device is added to the P2G to store excess H_2 when the renewable energy output is high, thus decoupling the electrolytic water and methanation procedures, while achieving the time shift of renewable energy power. The relationship between H_2 production by electrolytic water and H_2 consumption by methanation is as shown in Equation 13:

$$\begin{cases} V_{H_2,t} = V_{H_2,t}^{in} + V_{H_2,t}^{e-m} \\ V_{H_2,t}^m = V_{H_2,t}^{out} + V_{H_2,t}^{e-m} \end{cases} \tag{13}$$

Where, $V_{H_2,t}^{in}$, $V_{H_2,t}^{out}$ and $V_{H_2,t}^{e-m}$ represent H_2 from the electrolyzer into the hydrogen storage unit, from the hydrogen storage unit into the methane reactor, and directly from the electrolyzer into the methane reactor at time t, respectively. Suppose $V_{CH_4,t}^m$ represents CH_4 generated by P2G, then the ratio of $V_{C,t}^m$, $V_{H_2,t}^m$ and $V_{CH_4,t}^m$ is 1: 4:1.

(4) Gas storage devices

In this paper, both carbon storage devices and hydrogen storage devices are considered, which are used to decouple carbon capture, water electrolysis, and methanation procedures, maximize the absorption of wind power generation, and improve the degree of carbon recycling. In addition, the gas storage devices also require a high compression energy consumption. The operation modeling of the gas storage devices are shown as Equation 14:

$$\begin{cases} E_t = E_{t-1} + \eta_{in} V_t^{in} - \dfrac{V_t^{out}}{\eta_{out}} \\ g_{co,t} = \dfrac{\theta_{co} V_t^{in}}{3.6 \eta_{co}} \end{cases} \tag{14}$$

Where, E_t represents the gas stored at the time t; V_t^{in} and V_t^{out} represent the gas deposited and withdrawn at time t, respectively; η_{in} and η_{out} are the discharging and charging efficiency of the gas storage devices, respectively; $g_{co,t}$ is the compression energy dissipation at the time t; θ_{co} represents the compression energy consumption per unit gas; η_{co} indicates the working efficiency of the compressor.

3 Multi-objective stochastic dispatching optimization model of virtual power plant

Section 3 introduces the scheduling optimization model of virtual power plant. On the basis of the component model in Section 2, the optimal value of the decision variable is obtained through the objective function and some constraints.

3.1 Uncertainty scenario generation

This paper describes the uncertain factors of renewable energy output through the generation of uncertainty scenarios. In order to model the probability distribution of output power of fan and

photovoltaic, it is necessary to mine the information of historical data to directly model the uncertainty of output power. Currently, Latin hypercube sampling is the most common method for scene generation (Zhang et al., 2023; Ju et al., 2024), but this method ignores the correlation between the renewable energy output at different times. Therefore, in order to take into account the randomness and correlation of renewable energy output at all times, this paper proposes a scenario generation method considering the temporal correlation of wind power and PV output. The steps of this method are as follows:

(1) First, the covariance matrix $\sigma_{24 \times 24}$ of the full-cycle wind prediction error is constructed as shown in Equation 15:

$$\sigma_{ij} = \exp\left(-\frac{i-j}{\varepsilon}\right) \tag{15}$$

Where, σ_{ij} represents the covariance of time period i and time period j; ε is the key parameter of covariance, which is used to control the correlation strength.

(2) $Z_{1 \times 24} \sim N(0, \sigma_{24 \times 24})$ multivariate normal distribution of the full-cycle wind prediction error is constructed, and *mvnrnd* function in Matlab is called to generate N samples randomly.

(3) According to the probability distribution function in Section 1.2.1, the sample values of each period are inversely transformed to obtain the scenery prediction error, and then the corresponding N scenery output scenarios are calculated by Equation 2.

In order to reduce the amount of computation, this paper uses k-means clustering to reduce scenes to n typical scenes.

3.2 Multi-objective conventional dispatching optimization model

The objective functions of VPP conventional dispatching optimization model include minimum operating cost and minimum carbon emission.

(1) Minimum operating cost

The operating cost includes the power generation cost of CHP unit C_G, the maintenance and operation cost of various equipment C_M, the controllable load cost C_{DR} and the income from the buying and selling of electricity in the public grid I_{UG}. The calculation formula is shown in Equation 16.

$$\min F_1 = C_G + C_M + C_{DR} - I_{UG} \tag{16}$$

The power generation cost of CHP units includes fuel costs and start-up and shutdown costs, which are calculated as Equation 17:

$$C_G = \sum_{t=1}^{T} \left[c_{CH_4}\left(V_{CH_4,t} - V_{CH_4,t}^m\right) \right] + \sum_{t=1}^{T} c_{DT} |u_{c,t} - u_{c,t-1}| \tag{17}$$

Where, c_{CH_4} is the expense of natural gas; c_{DT} is the start-stop cost; $u_{c,t}$ is the start-stop variables of CHP at time t.

Operation and maintenance costs include the operating costs of wind power, photovoltaic, GPPCC, P2G, and electric boilers, which are calculated as Equation 18:

$$C_M = \sum_{t=1}^{T} \left[c_1 g_{WPP,t} + c_2 g_{PV,t} + c_3 g_{GPPCC,t} + c_4 \left(g_{H_2,t} + g_{CH_4,t}^m \right) + c_5 g_{eb,t} \right]$$

(18)

Where, c_1, c_2, c_3, c_4 and c_5 are the operating cost coefficients of wind power, photovoltaic, GPPCC, P2G, and electric boilers respectively.

Controllable load cost includes response output cost and standby output cost (Hao et al., 2023), which are calculated as Equation 19:

$$C_{DR} = \sum_{t=1}^{24} \sum_{k=1}^{N_I} \left(c_{I,k}^u \Delta L_{k,t}^u + c_{I,k}^d \Delta L_{k,t}^d + c_{R,k}^u R_{k,t}^u + c_{R,k}^d R_{k,t}^d \right)$$

(19)

Where, the cost factor of $c_{I,k}^u$ and $c_{I,k}^d$ providing positive/negative response power to the k user; $R_{k,t}^u$ and $R_{k,t}^d$ represent the positive/negative spare capacity that can be provided by the k th user; $c_{R,k}^u$ and $c_{R,k}^d$ provide positive/negative spare power cost factors for the k the user.

The income from the buying and selling of electricity for the public grid is calculated as Equation 20:

$$I_{UG} = \sum_{t=1}^{T} c_{UG,t} g_{UG,t}$$

(20)

Where, $c_{UG,t}$ is the electricity cost of the public grid; $g_{UG,t}$ is the amount of electricity sold (purchased) via the VPP to public grids.

(2) Minimum carbon footprint

Considering that China is still dominated by thermal power generation, this paper will also include the equivalent carbon emissions of electricity purchased in the public grid into the carbon emissions of VPP. The calculation formula is shown in Equation 21.

$$\min F_2 = \sum_{t=1}^{T} \left(Q_{c,t}^s - \eta_{UG} \min \left(g_{UG,t}, 0 \right) \right)$$

(21)

Where, η_{UG} is the carbon emission coefficient ever unit of electricity.

VPPs routine dispatching optimization model includes the following constraints:

(1) Electrical/thermal power balance constraint

In order to achieve the electricity/heat supply and demand balance of the VPP in each period, Equation 22 is established:

$$\begin{cases} g_{WPP,t} + g_{PV,t} + g_{Ge,t} + \Delta L_{I,t} = L_{e,t} + g_{GPPCC,t} \\ + g_{H_2,t} + g_{CH_4,t}^m + g_{co,t} + g_{eb,t} + g_{UG,t} \\ h_{G,t} + h_{eb,t} = L_{h,t} \end{cases}$$

(22)

(2) CHP unit output constraint

In order to limit the thermal and electrical output of CHP unit from exceeding its output range, Equation 23 is established:

$$\begin{cases} 0 \leq h_{G,i,t} \leq h_{G,i,\max} \\ s_{G,i,t} \max \left(g_{G,i,\min} - \eta_{eh,i} h_{G,i,t}, \alpha_i h_{G,i,t} + \beta_i \right) \leq g_{Ge,i,t} \leq s_{G,i,t} \left(g_{G,i,\max} - \eta_{eh,i} h_{G,i,t} \right) \\ \sum_{w=t}^{t+TS-1} (1 - u_{c,w}) \geq TS \left(u_{c,t-1} - u_{c,t} \right) \\ \sum_{w=t}^{t+TO-1} u_{c,w} \geq TO \left(u_{c,t} - u_{c,t-1} \right) \end{cases}$$

(23)

Where, $h_{G,i,\max}$ is the utmost value of thermal output; $g_{G,i,\max}$ and $g_{G,i,\min}$ are the greatest and least values of the total output; α_i is the elastic coefficient of electric power and thermal power; β_i is a constant; TS and TO are the minimum off/on time, respectively. Please refer to reference (Hao et al., 2023) for the specific climbing constraints of the unit.

(3) Controllable load constraint

In order to realize the reasonable transfer of controllable load, the transferable range is set. Therefore, Equation 24 is established:

$$\begin{cases} \mu_{k,t}^u \Delta L_{k,t}^u - \mu_{k,t}^d \Delta L_{k,t}^d + R_{k,t}^u \leq \Delta L_{k,\max} \\ \mu_{k,t}^u \Delta L_{k,t}^u - \mu_{k,t}^d \Delta L_{k,t}^d - R_{k,t}^d \leq \Delta L_{k,\max} \end{cases}$$

(24)

Where, $\Delta L_{k,\max}$ and $\Delta L_{k,\min}$ are the maximum positive/negative response forces that can be provided by the k th user.

(4) Equipment operation constraint

Similarly, GPPCC, P2G and other units also need to set their output ranges. Therefore, Equation 25 is established:

$$\begin{cases} g_{k,\min} \leq g_{k,t} \leq g_{k,\max} \\ -\Delta g_{k,d} \leq g_{k,t} - g_{k,t-1} \leq \Delta g_{k,u} \end{cases}$$

(25)

Where, $g_{k,\min}$ and $g_{k,\max}$ are the least and greatest operating power of type k equipment; $\Delta g_{k,u}$ and $\Delta g_{k,d}$ represent up/down climbing capability.

(5) Gas storage device constraint

The decision maker needs to consider the capacity limit and output range of the gas storage device, so Equation 26 is established:

$$\begin{cases} 0 \leq E_t \leq E_{\max} \\ 0 \leq V_t^{in} \leq s_t^{in} V_{\max}^{in} \\ 0 \leq V_t^{out} \leq s_t^{out} V_{\max}^{out} \\ 0 \leq s_t^{in} + s_t^{out} \leq 1 \\ E_0 = E_{24} \end{cases}$$

(26)

Where, $E_{\max}$ is the utmost gas storage volume of the gas storage devices; $V_{\max}^{in}$ and $V_{\max}^{out}$ are the maximum gas storage and venting rates; s_t^{in} and s_t^{out} are the status of gas storage and venting of gas storage devices, respectively.
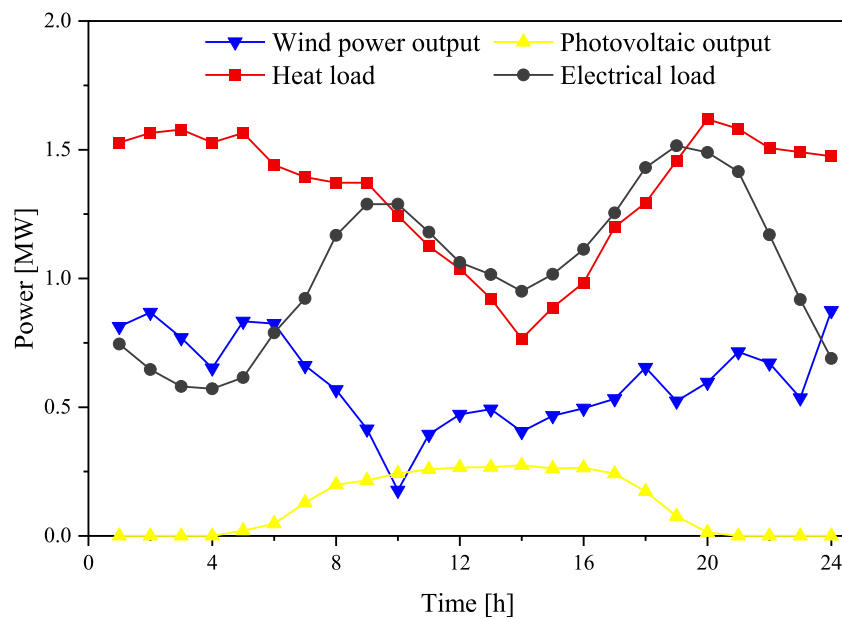
FIGURE 2
Forecasting wind power, photovoltaic power, power load, and heating load in the next day.

The conventional VPP scheduling model also includes system backup constraints, for details, please refer to Ref. (Zou et al., 2023).

3.3 Multi-objective stochastic dispatching optimization model

On the basis of value at risk (VaR), CVaR considers the risk distribution beyond the confidence level, and can reflect the maximum possible loss within the full probability interval of the portfolio under the given confidence degree. Therefore, this paper adopts CVaR theory to quantify the loss of load risk in real-time VPP scheduling, and takes it as an optimization target to reflect the operational risk of VPP, so as to cope with the incertitude of wind power generations. The approximate calculation formula of CVaR is as shown in Equation 27 (Ju et al., 2022):

$$\hat{F}_\beta(x, \alpha) = \alpha + \frac{1}{N(1-\beta)}\sum_{n=1}^{N}[f(x, y_n) - \alpha]^+ \quad (27)$$

Where, $f(x, y)$ is the loss function; x is the portfolio vector, y_n is the uncertainty scenario generated in Section 2.1; α and β represent VaR values and confidence levels; $[f(x, y) - \alpha]^+$ is equivalent to $\max(f(x, y) - \alpha, 0)$.

The measurement index of risk is often related to load loss and load loss duration (He et al., 2023), so this paper takes the loss penalty cost C_{ens} of VPP as the loss function, and the specific calculation is as shown in Equation 28:

$$C_{ens} = \sum_{t=1}^{T}c_{ens,t}\left(\Delta g_{WPP,t} + \Delta g_{PV,t} - R_t^u\right) \quad (28)$$

Where, $\Delta g_{WPP,t}$ and $\Delta g_{PV,t}$ are the deviation of the actual power generation of the scenery; $c_{ens,t}$ is the penalty cost coefficient of loss of load; R_t^u is the uplink standby capacity of VPP, which is mainly provided by the extraction steam unit, and the insufficient part is provided by the controllable load.

VPP multi-objective random dispatching optimization model is as shown in Equation 29:

$$\min F_1 = C_G + C_M + C_{DR} - I_{UG}$$

$$\min F_2 = \sum_{t=1}^{T}\left(Q_{c,t}^s - \eta_{UG}\min(g_{UG,t}, 0)\right) \quad (29)$$

$$\min F_{3,\beta} = \alpha + \frac{1}{N(1-\beta)}\sum_{k=1}^{N}\left(C_{risk}(G, g_k) - \alpha\right)$$

s.t. Equation 22 – 26

This section considers the uncertainty of new energy output, combined with the conventional VPP scheduling model, and then constructs the VPP multi-objective random scheduling optimization model. According to this idea, the decision maker can make the optimal VPP unit scheduling scheme.

4 Solving method of multi-objective model

In Section 4, according to the optimization model proposed in Section 3, the solution method of the optimization model is introduced.

TABLE 2 Weights of objectives in different cases.

Preference coefficient\scenario	Scenario 1		Scenario2		Scenario 3			Scenario4		
	F_1	F_2	F_1	F_2	F_1	F_2	F_3	F_1	F_2	F_3
0.1	0.65	0.35	0.66	0.34	0.53	0.31	0.16	0.53	0.30	0.17
0.2	0.63	0.37	0.65	0.35	0.51	0.32	0.17	0.52	0.30	0.18
0.3	0.60	0.40	0.64	0.36	0.50	0.33	0.17	0.51	0.31	0.19
0.4	0.58	0.42	0.63	0.37	0.49	0.34	0.18	0.50	0.31	0.20
0.5	0.56	0.44	0.62	0.38	0.47	0.34	0.18	0.49	0.31	0.21
0.6	0.53	0.47	0.61	0.39	0.46	0.35	0.18	0.48	0.31	0.22
0.7	0.51	0.49	0.59	0.41	0.45	0.36	0.19	0.46	0.31	0.23
0.8	0.49	0.51	0.58	0.42	0.44	0.37	0.19	0.45	0.31	0.24
0.9	0.46	0.54	0.57	0.43	0.42	0.38	0.20	0.44	0.31	0.25

TABLE 3 Optimization results of different cases under r = 0.1.

Scenario 1		Scenario 2			Scenario 3			Scenario 4			
F_1	F_2	F_1	F_2	m_{carbon}	F_1	F_2	F_3	F_1	F_2	m_{carbon}	F_3
10433.0	8945.6	10465.0	8328.6	265.8	10068.4	8690.5	43.3	9884.1	8132.4	342.7	63.0

4.1 Objective function dimensionality reduction

The three objective functions in this paper have different orders of magnitude, so the reduced semi-gradient membership function is used to de-dimensionalize. For the specific method, please refer to reference (Xuan et al., 2021). Membership function is as shown in Equation 30:

$$\pi(F_i) = \begin{cases} 0, F_i \geq F_i^{\max} \\ \dfrac{F_i^{\max} - F_i}{F_i^{\max} - F_i^{\min}}, F_i^{\min} \leq F_i \leq F_i^{\max} \\ 1, F_i \leq F_i^{\min} \end{cases} \qquad (30)$$

Where, F_i is the value of the i TH objective function; $F_i^{\min}$ and $F_i^{\max}$ are the least and greatest values of the objective function.

4.2 Subjective and objective integration weighting method

There are two kinds of weighting methods: subjective weighting and objective weighting. The results of subjective weighting depend heavily on the subjective knowledge of experts. The results of objective weighting may not necessarily represent the actual importance of the indicators (Song et al., 2020). Neither subjective weighting method nor objective

weighting method can perfectly reflect the importance of each objective function. Therefore, this paper chooses the analytic hierarchy process (AHP) as the subjective weighting method and the entropy weighting method as the objective weighting method. An integrated subjective and objective weighting method is proposed to assign weights to each optimization objective. Specific calculations are as shown in Equation 31:

$$w_i = \frac{u_i^r v_i^{1-r}}{\sum\limits_{i=1}^{3} u_i^r v_i^{1-r}}, i = 1, 2, 3 \qquad (31)$$

Where, w_i is the weighting obtained by assigning weight to subjective and objective integration; v_i and u_i are the weights obtained by analytic hierarchy procedure and entropy weight method; r is the preference coefficient of decision makers for subjective and objective factors, with the value between 0 and 1.

4.3 Model solution

After the objective function is de-dimensional and weighted by subjective and objective integration, Equation 29 can be converted into the form of Equation 32, and the result of VPP multi-objective scheduling optimization can be obtained by solving it. In addition, the first item of Equation 8 needs to be linearized.

$$\min f = \sum_{i=1}^{3} w_i \pi(F_i) \qquad (32)$$
$$s.t \quad \text{Equation} \quad 22 - 26.$$

5 Example analysis

5.1 Example data

For the purpose of this paper, the VPP of a certain place in China is selected as the simulation object, VPP has two 0.8 MW CHP units with a combined capacity of 1 MW for wind and 0.4 MW for PV, a capacity of 0.15 MW for electric boilers, and a maximum response output of 0.03 MW for controllable loads. The penalty cost coefficient of loss of load is 800 yuan/MW, the confidence is 0.8, and the power upper limit of VPP interacting with the grid is set to 0.1 MW. Figure 2 shows the predicted next-day wind power and electric heating load. It can be seen that the scene generation method takes into account the randomness and correlation of the output of the scenery at every moment, and is more in line with the actual output of the scenery. In this paper, examples are simulated on Matlab R2016a. The time spent in generating and reducing uncertain scenes is about 5s, and the results can be obtained within 15s for model solving.

5.2 Scenario setting

In order to analyze the carbon recycling capability of GPPCC and P2G and the effectiveness of the uncertainty coping method, the following four scenarios are set for simulation analysis.

Scenario 1: Basic scenario. GPPCC and P2G were not introduced, and the uncertainty coping method in this paper was not adopted.

Scenario 2: Carbon recycling scenario. GPPCC and P2G were introduced, but uncertainty coping methods were not adopted.

Scenario 3: Risk avoidance scenario. The uncertainty coping method was adopted, but GPPCC and P2G were not introduced.

Scenario 4: Integrated scenario. Both GPPCC and P2G are introduced, and uncertainty coping methods are adopted.

5.3 Example result

Firstly, the entropy weight method and analytic hierarchy procedure were used to calculate the weight of the objective function under each scenario. Then, the sensitivity analysis of decision-maker's subjective and objective factor preference coefficient is carried out, and the weight of subjective and objective integration was calculated according to Equation 31, as shown in Table 2.

It can be seen that when r gradually increases, the weight of running cost F_1 gradually decreases. In addition, the weight of carbon emission F_2 and risk cost F_3 are gradually
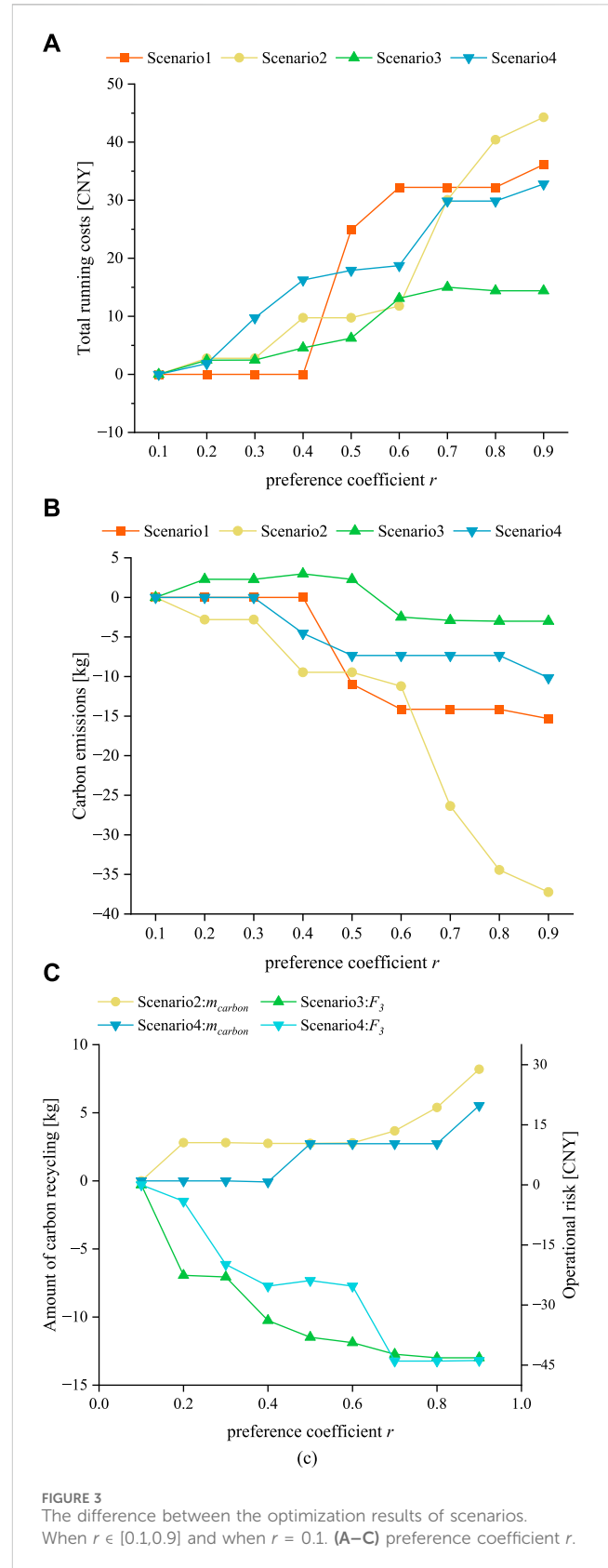

FIGURE 3
The difference between the optimization results of scenarios. When $r \in [0.1, 0.9]$ and when $r = 0.1$. (A–C) preference coefficient r.

increasing. This is because when r is small, the subjective weight has more influence, and the subjective weighting method pays more attention to the impact of operating costs
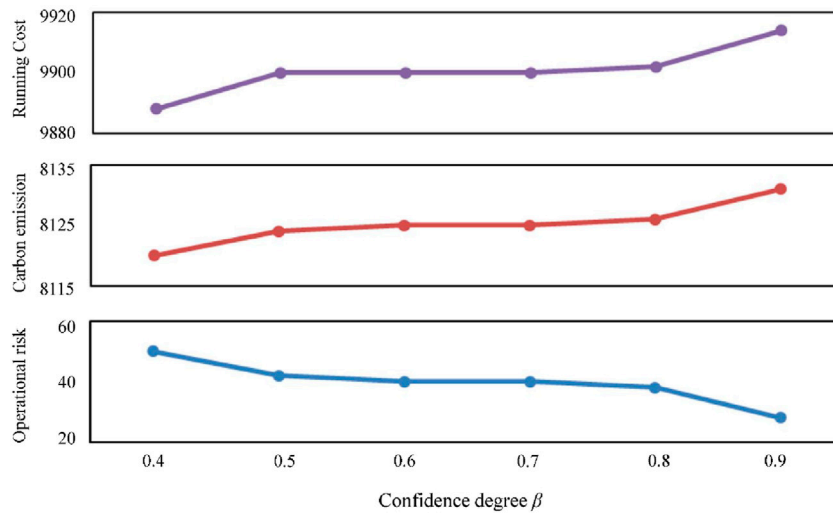
FIGURE 4
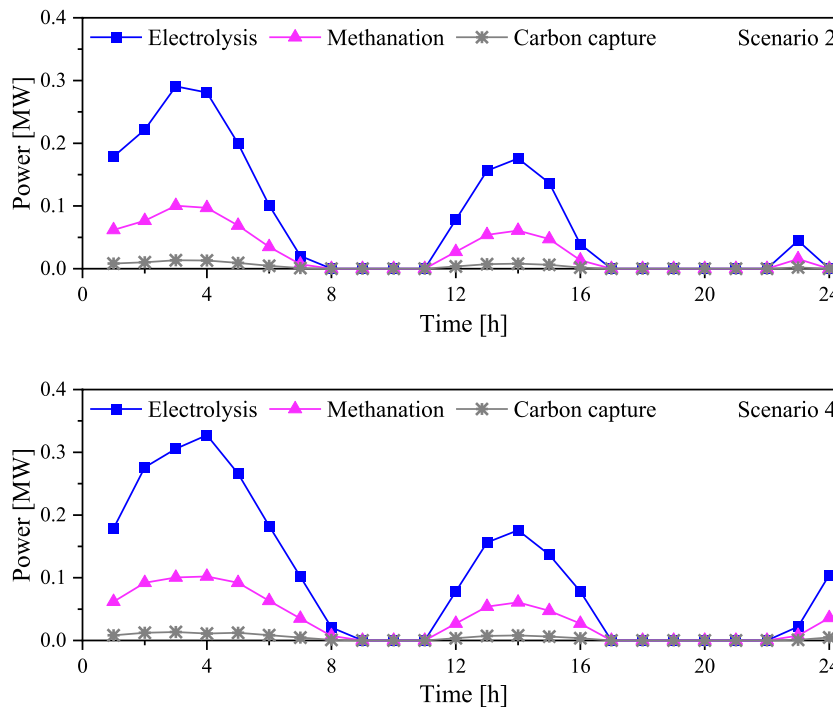Objective values with different β in case 4.

FIGURE 5
Operating power of different units in case 2 and case 4.

on the system. It is worth pointing out that in Scenario 2-4, F_1 is the most weighted optimization target regardless of how r changes. This also reflects the importance of running costs to the entire system.

Table 3 shows the optimization results of scenarios when $r = 0.1$, and Figure 3 shows the difference between the optimization results of scenarios when $r \in [0.1, 0.9]$ and when $r = 0.1$. In the legend of Figure 3C, m_{carbon} refers to the amount of carbon

recycling. Combined with Table 3 and Figure 3, a comparative analysis of each scenario is carried out: In Scenario 2, compared with Scenario 1, the addition of carbon recycling devices increases the overall cost slightly, but the carbon emissions decrease significantly, by about 7%. In Scenario 3, compared with Scenario 1, the uncertainty coping method proposed in this paper reduces the overall cost by about 3.5%. In addition, carbon emissions are also reduced, by about 3%. In

FIGURE 6
Operating power of P2G with different additional reserve capacity.
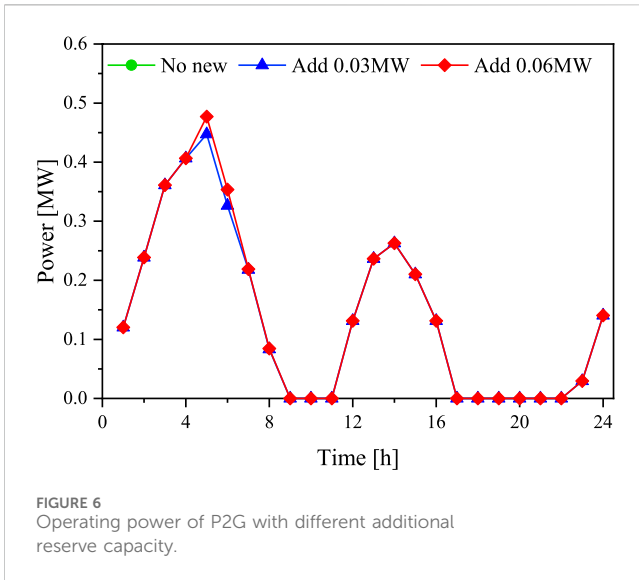
comparison with Scenario 2 and Scenario 3, the use of the comprehensive method makes the operating cost and carbon emission of Scenario 4 the lowest value among the four scenarios, and the carbon recovery amount of Scenario 4 is

higher than that of Scenario 2. To sum up, adding carbon cycle device can greatly improve the environmental benefit; The use of CVaR method can greatly improve the economic benefit. Using a comprehensive approach is more effective than using a single approach.

In addition, the relationship between the value of the objective function and r can be analyzed from Figure 3. With the increase of r, the weight of F_1 decreases, while the weight of F_2 and F_3 increases. Therefore, the operation cost of each scenario gradually increases, and the carbon emission and risk cost overall show a downward trend. In addition, for Scenario 2 and Scenario 4 where carbon recovery exists, the amount of carbon recovery increases significantly, with an increase ratio of 3.08% and 1.61% respectively. For Scenario 3 and 4 with risk cost, as r increases from 0.1 to 0.9, F_3 decreases by 99.7% and 69.53% in Scenario 3 and 4, respectively.

According to the results of the sensitivity analysis in Figure 3, when the value of r is centered, the importance distribution of each objective in VPP is more balanced: VPP neither attaches too much importance to operational risks nor ignores carbon recycling. Therefore, in order to compare the results of different scenarios more conveniently, the results when the subjective and objective factor preference coefficient r is 0.5 are selected for further analysis.

TABLE 4 Recycled carbon quantity before and after adding gas storage devices.

	No gas storage is added	Add carbon storage device	Add hydrogen storage device	Add carbon storage and hydrogen storage devices
Carbon cycle amount (m^3)	345.38	357.59	366.57	378.05

FIGURE 7
Operating power and stored gas quantity after adding carbon storage or hydrogen storage devices.
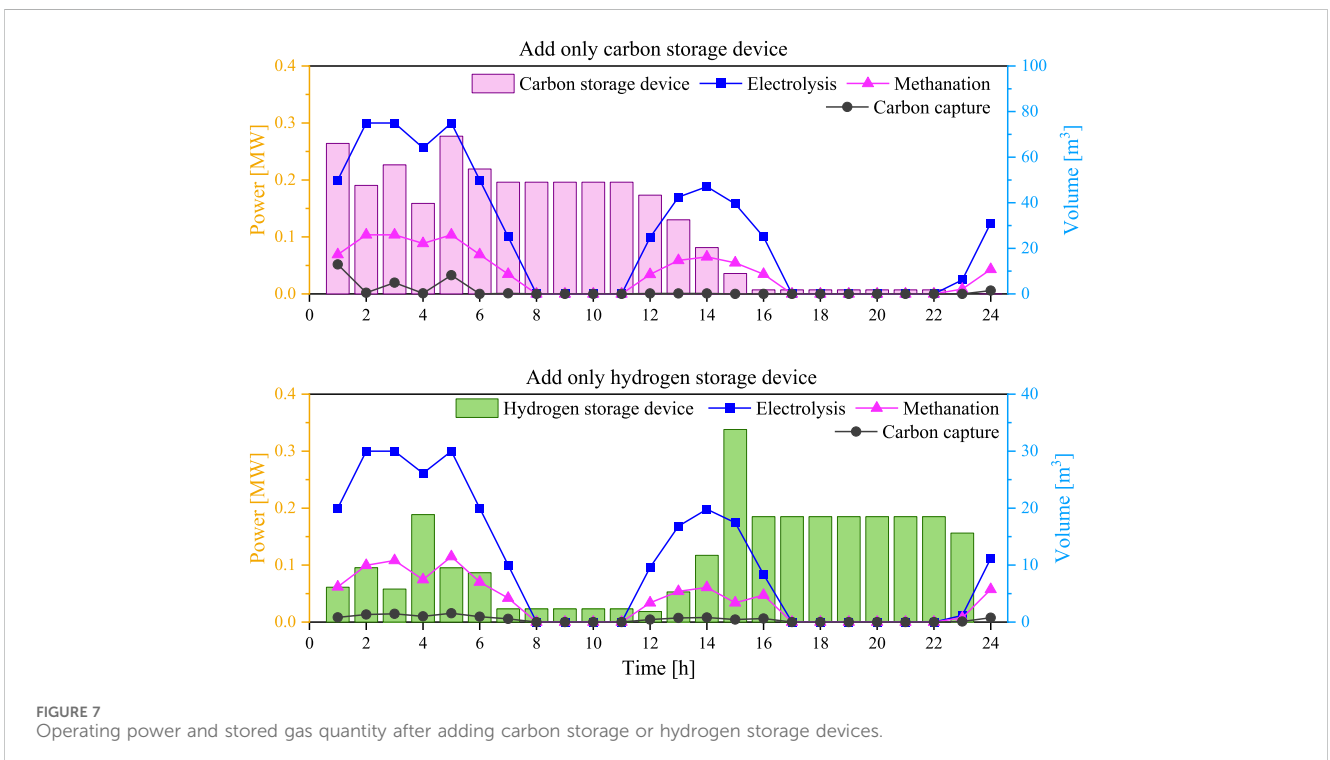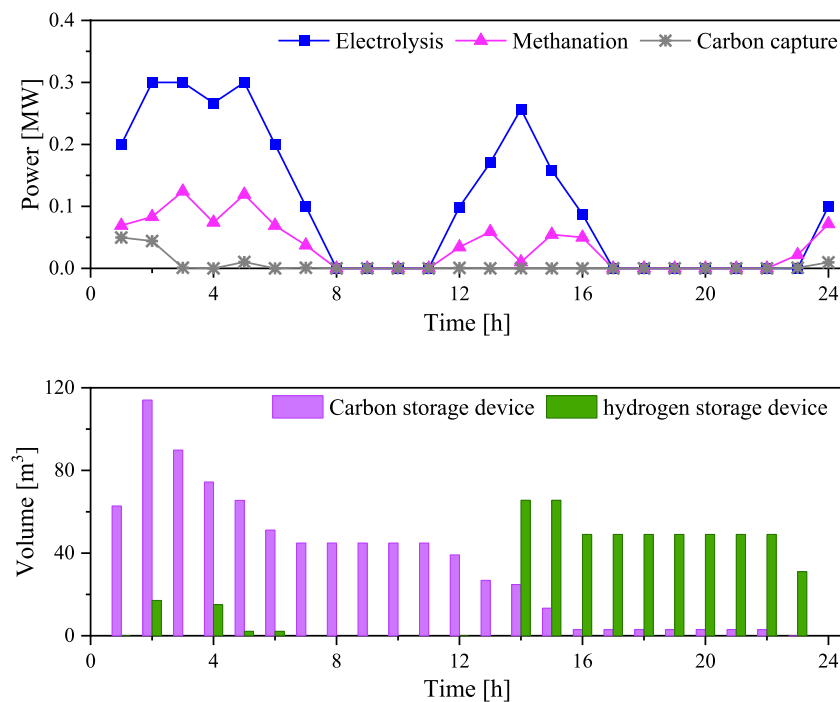
FIGURE 8
Operating power and stored gas quantity after adding carbon storage and hydrogen storage devices.

5.3.1 Analysis on the effectiveness of uncertainty coping methods

As shown in Figure 3 ($r = 0.5$), compared with Scenario 1 and Scenario 2, Scenario 3 and Scenario 4 adopted the uncertainty coping method in this paper, and the operating cost was reduced by 383.21CNYand 572.76CNY, the carbon emission was reduced by 241.91 kg and 194.11 kg, respectively, but the operating risk was increased by 5.27CNYand 39.17CNY.

As can be seen, Scenario 1 and Scenario 2 adopt the conventional system reserve constraint and arrange the reserve capacity according to the fixed proportion of the wind-view planned output. Scenario 3 and Scenario 4 adopt the uncertainty coping method in this paper, which can fully consider the real-time risk situation, arrange more planned output for wind power in periods 7–8, 17–18, and 21–22, and bear certain risks to gain greater benefits. In addition, compared with Scenario 1 and Scenario 2, Scenario 3 and Scenario 4 have generally lower controllable load backup output, which saves part of the backup cost for VPP. The above analysis shows that the uncertainty coping method in this paper can fully measure the risk situation in real-time scheduling, and arrange wind power generation plan and backup plan more reasonably so that VPP can obtain more benefits while avoiding risks in real-time scheduling. Figure 4 shows the target values under different confidence levels in Scenario 4.

As shown in Figure 4, with the increase in confidence, the attitude of decision-makers gradually becomes conservative, resulting in a gradual increase in operating costs and carbon emissions, and a gradual decrease in operating risks. When $0.5 \le \beta \le 0.8$, the change of operating cost and operating risk is relatively gentle, the sensitivity of the model to risk is weak; When $0.4 \le \beta \le 0.5$ or $0.8 \le \beta \le 0.9$, the change of operating cost and

operating risk is relatively large, indicating that the model is more sensitive to risk.

5.3.2 GPPCC and P2G carbon recycling capacity analysis

As shown in Figure 3 ($r = 0.5$), compared with Scenario 1, Scenario 2 recycled 268.54 kg, carbon emission decreased by 615.49 kg, and operation cost increased by 16.87CNY, which greatly improved the environmental protection of VPP at the cost of a certain economic loss. Compared with scenario 3, scenario 4 recycle 345.38 kg of CO_2, reduces carbon emissions by 567.69 kg, reduces operating costs by 172.68CNY, and improves the economy and environmental protection of VPP. Figure 5 shows the operating power of water electrolysis, methanation, and carbon capture units in scenarios 2 and 4.

It can be seen that during periods 1–7, 12–16, and 23–24, GPPCC and P2G will use surplus renewable energy to generate electricity and realize the recycling of CO_2. Among them, Scenario 4, due to the uncertainty coping method, can fully measure the risks in real-time operation of VPP, and choose to absorb more wind power generation to improve economic and environmental benefits, such as periods 4–7 and 13–16. In addition, in both Scenario 2 and Scenario 4, GPPCC and P2G do not reach their maximum operating power, because the limited backup provided by CHP units and controllable loads prevents GPPCC and P2G from generating a high percentage of wind power. Figure 6 shows the running power of P2G in scenario 4 under different new spares.

As can be seen from Figure 6, with the boost of spare capacity, the operating power of P2G at periods 5–8 and 13–15 keeps rising, indicating that the carbon recycling capacity of GPPCC and P2G is limited by the spare capacity of VPP, and seeking new spare

resources within VPP will be the key to improve the carbon recycling degree of GPPCC and P2G.

5.3.3 Analysis on the degree of carbon recycling improved by gas storage devices

According to Figure 6, in conventional carbon cycle modeling, carbon capture, water electrolysis, and methanation operate in a coupled manner, which cannot maximize the recycling of CO_2. Carbon storage device and hydrogen storage device are now added, and the initial gas storage is set to 0 m^3 and 50 m^3 respectively (standard condition). Table 4 shows the carbon cycle utilization before and after adding the gas storage device. It can be seen that when the carbon storage device and hydrogen storage device are added at the same time, the carbon cycle utilization is increased by 32.67 m^3, and the degree of carbon recycling is increased by 9.46%, which is 20.46 m^3 and 11.48 m^3 more than that when only the carbon storage device or hydrogen storage device is added. Figures 7, 8 respectively show the operating power and storage capacity when only carbon storage device or hydrogen storage device is added and the operating power and storage capacity when two gas storage devices are added.

As shown in Figure 7, the carbon storage device can realize the decoupling of carbon capture and methanation procedures, storing excess CO_2, at periods 1 and 5, and converting it into CH_4 at periods 11–15. Although the degree of carbon recycling has been improved to some extent, the electrolysis of water and methanation still operate in a coupled manner, and the surplus of renewable energy generation cannot be fully utilized. The hydrogen storage device can realize the decoupling of electrolytic water and methanation procedure, generate and store H_2 by using surplus renewable energy generation in periods 4 and 12–14, and consume it in periods 4–7 and 23–24 to achieve the time shift of renewable energy power. The degree of carbon recycling is also improved to a certain extent, but carbon capture and methanation still operate in a coupling manner, unable to make full use of CO_2 during the entire scheduling cycle.

As shown in Figure 8, water electrolysis, methanation, and carbon capture all operate in a decoupled manner when both carbon and hydrogen storage devices are added. The carbon storage device mainly stores excess CO_2 at periods 1-2, and the hydrogen storage device mainly stores excess H_2 at periods 4 and 14–15. The combined use of the two gas storage devices can not only effectively use the CO_2 generated during the whole dispatching cycle, but also realize the time shift of renewable energy power with H_2 as the medium, and maximize the carbon recycling degree of GPPCC and P2G. At this time, the average energy utilization efficiency of VPP as a whole is about 94.17%. Among them, the average energy use efficiency of renewable energy is only 71.22%. It can be seen that although carbon capture and power to gas devices can use surplus renewable energy electricity to achieve CO_2 recycling, the energy loss caused by this procedure needs to be further optimized.

6 Conclusion

In this paper, GPPCC and P2G are introduced into a combined heat and power virtual power plant to achieve CO_2 recycling, and carbon storage devices and hydrogen storage devices are added to

decouple carbon capture and P2G procedures. Then, the uncertainty scenario generation and CVaR theory are used to quantify the risk of load loss in VPP real-time scheduling, and the multi-objective stochastic dispatching optimization model of the virtual power plant is constructed with the target of operating cost, carbon emission, and operating risk. Finally, the validity and applicability of the model are verified by a design example, and the conclusions are as follows:

(1) The uncertainty analysis method in this paper can fully measure the risk situation in real-time scheduling, and arrange wind power generation plan and backup plans more reasonably so that VPP can obtain more benefits while avoiding risks in real-time scheduling.

(2) The GPPCC and P2G combined carbon and hydrogen storage devices can flexibly control the production and consumption of CO_2 and H_2, and effectively decouple the carbon capture, water electrolysis and methanation processes. At the same time, the time shift of renewable energy power is realized, thus maximizing the degree of carbon recovery. The example analysis shows that the carbon cycle degree increases by 9.46% when carbon storage device and hydrogen storage device are added at the same time.

(3) Combined carbon recycling and risk avoidance, the result of operation is better than only one measure. In Scenario 4, the total operating cost and carbon emissions are reduced by 555.89 CNY and 809.6 kg, respectively, and the VPP energy utilization efficiency reaches 94.17%.

In the future, with the continuous maturity of carbon cycle technology, CHP units, GPPCC and P2G modules will effectively improve the efficiency of CHP virtual power plants. Meanwhile, new power generation resources will be added to the VPP, such as solar thermal electric plants, electro hydrogen coupling systems, etc. Which will further improve the efficiency of VPP.

Data availability statement

The original contributions presented in the study are included in the article/supplementary material, further inquiries can be directed to the corresponding author.

Author contributions

FZ: Visualization, Writing–review and editing. YG: Visualization, Writing–review and editing. XZ: Investigation, Writing–original draft. FL: Investigation, Writing–original draft. QZ: Validation, Writing–original draft.

Funding

involved in the study design, collection, analysis, interpretation of data, the writing of this article, or the decision to submit it for publication.

Conflict of interest

Authors FZ and YG were employed by State Grid Energy Research Institute Co., Ltd. Author XZ and FL were employed by State Grid Qinghai Electric Power Company.

The remaining authors declare that the research was conducted in the absence of any commercial or financial relationships that could be construed as a potential conflict of interest.

Publisher's note

All claims expressed in this article are solely those of the authors and do not necessarily represent those of their affiliated organizations, or those of the publisher, the editors and the reviewers. Any product that may be evaluated in this article, or claim that may be made by its manufacturer, is not guaranteed or endorsed by the publisher.

References

Babaee, S., and Loughlin, D. H. (2018). Exploring the role of natural gas power plants with carbon capture and storage as a bridge to a low-carbon future. *Clean Technol. Environ. policy* 20 (2), 379–391. doi:10.1007/s10098-017-1479-x

Banadkouki, M. R. Z. (2023). Selection of strategies to improve energy efficiency in industry: a hybrid approach using entropy weight method and fuzzy TOPSIS. *Energy* 279, 128070. doi:10.1016/j.energy.2023.128070

Bassano, C., Deiana, P., Vilardi, G., and Verdone, N. (2020). Modeling and economic evaluation of carbon capture and storage technologies integrated into synthetic natural gas and power-to-gas plants. *Appl. Energy* 263, 114590. doi:10.1016/j.apenergy.2020.114590

Basu, M. (2023). Optimal day-ahead scheduling of renewable energy-based virtual power plant considering electrical, thermal and cooling energy. *J. Energy Storage* 65, 107363. doi:10.1016/j.est.2023.107363

De Giorgi, M. G., Congedo, P. M., Malvoni, M., and Laforgia, D. Error analysis of hybrid photovoltaic power forecasting models: a case study of mediterranean climate[J]. *Energy Convers. Manag.*, 2015, 100: 117–130. doi:10.1016/j.enconman.2015.04.078

Feng, Y., Jia, H., Wang, X., Ning, B., Liu, Z., and Liu, D. (2023). Review of operations for multi-energy coupled virtual power plants participating in electricity market. *Energy Rep.* 9, 992–999. doi:10.1016/j.egyr.2023.04.149

Gorre, J., Ruoss, F., Karjunen, H., Schaffert, J., and Tynjälä, T. (2020). Cost benefits of optimizing hydrogen storage and methanation capacities for Power-to-Gas plants in dynamic operation. *Appl. Energy* 257, 113967. doi:10.1016/j.apenergy.2019.113967

Hao, J., Zheng, P., Li, Y., Zhang, Z., Zhang, J., Yang, J., et al. (2023). Study on the operational feasibility domain of combined heat and power generation system based on compressed carbon dioxide energy storage. *Energy* 291, 130122. doi:10.1016/j.energy.2023.130122

He, S., Gao, H., Chen, Z., and Liu, J. (2023). Data-driven worst conditional value at risk energy management model of energy station. *Energy* 266, 126421. doi:10.1016/j.energy.2022.126421

Higgins, P., Foley, A. M., Douglas, R., and Li, K. (2014). Impact of offshore wind power forecast error in a carbon constraint electricity market. *Energy* 76, 187–197. doi:10.1016/j.energy.2014.06.037

Ju, L., Bai, X., Li, G., Gan, W., Qi, X., and Ye, F. (2024). Two-stage robust transaction optimization model and benefit allocation strategy for new energy power stations with shared energy storage considering green certificate and virtual energy storage mode. *Appl. Energy* 362, 122996. doi:10.1016/j.apenergy.2024.122996

Ju, L., Zhao, R., Tan, Q., Lu, Y., and Wang, W. (2019). A multi-objective robust scheduling model and solution algorithm for a novel virtual power plant connected with power-to-gas and gas storage tank considering uncertainty and demand response. *Appl. Energy* 250, 1336–1355. doi:10.1016/j.apenergy.2019.05.027

Ju, L. W., Yin, Z., Lu, X. L., Yang, S., and Rao, R. (2022). A Tri-dimensional Equilibrium-based stochastic optimal dispatching model for a novel virtual power plant incorporating carbon Capture, Power-to-Gas and electric vehicle aggregator. *Appl. Energy* 324, 119776. doi:10.1016/j.apenergy.2022.119776

Marzi, E., Morini, M., Saletti, C., Vouros, S., Zaccaria, V., Kyprianidis, K., et al. (2023). Power-to-Gas for energy system flexibility under uncertainty in demand, production and price. *Energy* 284, 129212. doi:10.1016/j.energy.2023.129212

Nazari-Heris, M., Madadi, S., and Abapour, S. Optimal stochastic scheduling of virtual power plant considering NaS battery storage and combined heat and power units [J]. *J. Energy Manag. Technol.*, 2018, 2(3): 1–7. doi:10.22109/jemt.2018.133447.1095

Schulz, C., Roder, G., and Kurrat, M. (2005) "Virtual power plants with combined heat and power micro-units," in 2005 international conference on future power systems. Amsterdam, Netherlands: IEEE, 5.

Smit, B., Park, A. H. A., and Gadikota, G. 2014, The grand challenges in carbon capture, utilization, and storage. *Front. Energy Res.*: 55, doi:10.3389/fenrg.2014.00055

Song, X., Zhao, R., De, G., Wu, J., Shen, H., Tan, Z., et al. (2020). A fuzzy-based multi-objective robust optimization model for a regional hybrid energy system considering uncertainty. *Energy Sci. Eng.* 8 (4), 926–943. doi:10.1002/ese3.674

Tan, C., Wang, J., Geng, S., and Tan, Z. (2021). Three-level market optimization model of virtual power plant with carbon capture equipment considering copula–CVaR theory. *Energy* 237, 121620. doi:10.1016/j.energy.2021.121620

Wang, C., Wang, H., Ji, X., Xu, H., Yang, C., and Meng, X. (2024). Hybrid energy storage capacity configuration strategy for virtual power plants based on variable-ratio natural gas-hydrogen blending. *Int. J. Hydrogen Energy* 58, 433–445. doi:10.1016/j.ijhydene.2024.01.175

Xia, Y., Liu, J., Huang, Z., and Zhang, X. (2016). Carbon emission impact on the operation of virtual power plant with combined heat and power system. *Front. Inf. Technol. Electron. Eng.* 17, 479–488. doi:10.1631/fitee.1500467

Xuan, A., Shen, X., Guo, Q., and Sun, H. (2021). A conditional value-at-risk based planning model for integrated energy system with energy storage and renewables. *Appl. Energy* 294, 116971. doi:10.1016/j.apenergy.2021.116971

Yang, H., Tian, X., Liu, F., Liu, L., Li, L., and Wang, Q. (2024). A multi-objective dispatching model for a novel virtual power plant considering combined heat and power units, carbon recycling utilization, and flexible load response. *Front. Energy Res.* 11, 1332474. doi:10.3389/fenrg.2023.1332474

Yang, Y., Li, Z., Mandapaka, P. V., and Lo, E. Y. (2023). Risk-averse restoration of coupled power and water systems with small pumped-hydro storage and stochastic rooftop renewables. *Appl. Energy* 339, 120953. doi:10.1016/j.apenergy.2023.120953

Zhang, S., Gu, W., Wang, J., Zhang, X.-P., Meng, X., Lu, S., et al. (2024). Steady-state security region of integrated energy system considering thermal dynamics. *IEEE Trans. Power Syst.* 39, 4138–4153. doi:10.1109/tpwrs.2023.3296080

Zhang, S., Gu, W., Zhang, X.-P., Lu, H., Lu, S., Yu, R., et al. (2022). Fully analytical model of heating networks for integrated energy systems. *Appl. Energy* 327, 120081. doi:10.1016/j.apenergy.2022.120081

Zhang, Y., Pan, Z., Wang, H., Wang, J., Zhao, Z., and Wang, F. (2023). Achieving wind power and photovoltaic power prediction: an intelligent prediction system based on a deep learning approach. *Energy* 283, 129005. doi:10.1016/j.energy.2023.129005

Zhu, C., Bao, G., Xu, R., Song, Z., and Liu, Y. (2023). Low-carbon economic analysis of a virtual power plant with wind and solar power considering the integrated flexible operation mode of a carbon capture thermoelectric unit. *Int. J. Greenh. Gas Control* 130, 104011. doi:10.1016/j.ijggc.2023.104011

Zou, D., Gong, D., and Ouyang, H. (2023). The dynamic economic emission dispatch of the combined heat and power system integrated with a wind farm and a photovoltaic plant. *Appl. Energy* 351, 121890. doi:10.1016/j.apenergy.2023.121890

Nomenclature

Abbreviations

VPP	virtual power plants
CHP	combined heat and power
CHP-VPP	combined heat and power-virtual power plant
P2G	Power-to-gas
GPPCC	Gas-power Plant Carbon Capture
CVaR	Conditional Value-at-Risk
PV	Photovoltaic

Sets

t	index for time
k	index for user
i, j	index for time period

Scalars

ω_{eb}	electric heating efficiency of the electric boiler
k_m, k_u	minimum and maximum thermoelectric ratio of CHP
e_G	carbon emission intensity
η_G	power generation efficiency of CHP unit
H_{CH_4}	low calorific value of natural gas
$\lambda_{c,t}$	flue gas diversion ratio at time t
η_c	constant representing the CO_2 capture rate of GPPCC
θ_{ce}	power consumed per unit of CO_2
ρ_c	density of CO_2 under the standard condition
η_{H_2}	efficiency of converting electricity to hydrogen
H_{H_2}	calorific value of hydrogen
$\theta_{CH_4}^m$	power consumption per unit H_2 of methanation consumption
η_{in}, η_{out}	discharging and charging efficiency of the gas storage devices
θ_{co}	compression energy consumption per unit gas
η_{co}	working efficiency of the compressor
η_{UG}	carbon emission coefficient ever unit of electricity

Parameter

$g_{WPP,t}$	planned output of wind power at time t
$g_{WPP,t}^f$	predicted output of wind power at time t
$g_{WPP,t}^{re}$	actual output of wind power at time t
$\Delta g_{WPP,t}^f$	forecast error of wind power at time t
W_{WPP}	total installed cubage of wind turbines
$\Delta L_{I,t}$	controllable load response quantity at time t
N_I	number of users
$\Delta L_{k,t}^u, \Delta L_{k,t}^d$	positive/negative response provided by the k user
$\mu_{k,t}^u, \mu_{k,t}^d$	state of the positive/negative response force
P_{CHP}	power of CHP rated electric

C_{CHP}^e, C_{CHP}^h	rated electric thermal power of CHP unit
ϕ_{CHP}	thermal power of CHP

Variables

$h_{eb,t}$	heat production power of electric boilers at time t
$g_{eb,t}$	power consumption power of electric boilers at time t
$Q_{G,c,t}$	mass of CO_2 produced by CHP at time t
$V_{CH_4,t}$	volume of natural gas consumed by CHP at time t
$g_{OP,t}$	operation energy consumption at time t
$g_{G,t}$	the total electrical power of CHP at time t
$Q_{c,t}, Q_{c,t}^c, Q_{c,t}^g$	CO_2 being processed, successfully captured, and released into the atmosphere by GPPCC
g_A	fixed energy absorbed of carbon capture
$V_{c,t}^c$	volume of CO_2 being successfully captured
$V_{c,t}^{in}, V_{c,t}^{out}, V_{c,t}^{c-m}$	CO_2 from GPPCC into the carbon storage unit, from the carbon storage unit into P2G, and directly from GPPCC into P2G
$V_{c,t}^m$	total amount consumed by P2G
$V_{H_2,t}, V_{H_2,t}^m$	H_2 produced by electrolytic water and consumed by methanation
$g_{H_2,t}, g_{CH_4,t}^m$	power consumption of water electrolysis and methanation
$V_{H_2,t}^{in}, V_{H_2,t}^{out}$	H_2 from the electrolyzer into the hydrogen storage unit, from the hydrogen storage unit into the methane reactor at time t
$V_{H_2,t}^{e-m}$	H_2 directly from the electrolyzer into the methane reactor at time t
$V_{CH_4,t}^m$	CH_4 generated by P2G
E_t	gas stored at the time t
V_t^{in}, V_t^{out}	gas deposited and withdrawn at time t
$g_{co,t}$	compression energy dissipation at time t
C_G	power generation cost of CHP unit
C_M	maintenance and operation cost of various equipment
C_{DR}	controllable load cost
I_{UG}	income from the buying and selling of electricity in the public grid
c_{CH_4}	expense of natural gas
c_{DT}	start-stop cost
$u_{c,t}$	start-stop variables of CHP at time t
c_1, c_2, c_3, c_4, c_5	operating cost coefficients of wind power, photovoltaic, GPPCC, P2G, and electric boilers
$c_{I,k}^u, c_{I,k}^d$	providing positive/negative response power to the k user
$R_{k,t}^u, R_{k,t}^d$	positive/negative spare capacity that can be provided by the k th user
$c_{R,k}^u, c_{R,k}^d$	provide positive/negative spare power cost factors for the k the user
$c_{UG,t}$	electricity cost of the public grid
$g_{UG,t}$	amount of electricity sold (purchased) via the VPP to public grids
F_1	operating cost
F_2	carbon footprint
$h_{G,i,\max}$	utmost value of thermal output

$g_{G,i,\max}$, $g_{G,i,\min}$	greatest and least values of the total output
α_i	elastic coefficient of electric power and thermal power
β_i	a constant
TS, TO	minimum off/on time
$\Delta L_{k,\max}$, $\Delta L_{k,\min}$	maximum positive/negative response forces that can be provided by the k th user
$g_{k,\min}$, $g_{k,\max}$	least and greatest operating power of type k equipment
$\Delta g_{k,u}$, $\Delta g_{k,d}$	up/down climbing capability
$E_{\max}$	utmost gas storage volume of the gas storage devices
$V_{\max}^{in}$, $V_{\max}^{out}$	maximum gas storage and venting rates
s_t^{in}, s_t^{out}	status of gas storage and venting of gas storage devices
C_{ens}	loss penalty cost
$\Delta g_{WPP,t}$, $\Delta g_{PV,t}$	deviation of the actual power generation of the scenery
$c_{ens,t}$	penalty cost coefficient of loss of load
R_t^u	uplink standby capacity of VPP
F_i	value of the i TH objective function
$F_i^{\min}$, $F_i^{\max}$	least and greatest values of the objective function

Algorithm

σ_{ij}	covariance of time period i and time period j
ε	key parameter of covariance
N	number of random samples
n	number of typical scenes
$f(x,y)$	loss function
x	portfolio vector
y_n	uncertainty scenario generated in Section 2.1
α, β	VaR values and confidence levels
w_i	weighting obtained by assigning weight to subjective and objective integration
v_i, u_i	weights obtained by analytic hierarchy procedure and entropy weight method
r	preference coefficient of decision makers for subjective and objective factors